International Journal of Nanomedicine

Dovepress
open access to scientific and medical research

Open Access Full Text Article

ORIGINAL RESEARCH

Preparation and in vitro and in vivo Study of Asiaticoside-Loaded Nanoemulsions and Nanoemulsions-Based Gels for Transdermal Delivery

This article was published in the following Dove Press journal:
International Journal of Nanomedicine

Huimin Li[1,*]
Qian Peng[2,*]
Yisha Guo[3]
Xiaohui Wang[1]
Li Zhang[1]

[1]Department of Pharmacy, Logistics College of Chinese People's Armed Police Forces, Tianjin 300309, People's Republic of China; [2]Jiangsu Hengrui Pharmaceutical Co. LTD, Jiangsu 222000, People's Republic of China; [3]Characteristic Medical Center of the Chinese People's Armed Police Forces, Tianjin 300162, People's Republic of China

*These authors contributed equally to this work

Purpose: Asiaticoside (ASI), a compound of triterpene pentacyclic saponins, has apparently therapeutic efficacy on human hypertrophic scar. However, the characteristics of large molecular weight, low water solubility and poor lipophilicity do not favor the diffusion through the stratum corneum (SC). Therefore, it is expected that the development of a transdermally delivered formulation may enhance the permeability ratio (Qn) of ASI for its clinical application. In this study, we designed asiaticoside-loaded nanoemulsions (ASI-NEs) and nanoemulsions-based gels (ASI-NBGs) and studied their mechanism for transdermal delivery.

Methods: The preparation of ASI-NEs was optimized by simplex lattice design (SLD). The ex vivo transdermal penetration and the in vivo pharmacokinetics studies were studied, respectively. The skin irritation of ASI-NEs and ASI-NBGs was measured on normal and damaged skin in rabbits, and the transcutaneous mechanisms of ASI-NEs and ASI-NBGs were determined by HE stained and confocal laser scanning microscopy (CLSM).

Results: The mean particle size of ASI-NEs was 132±5.84nm. The ex vivo skin permeation study verified that the Qn of the optimized ASI-NEs and ASI-NBGs was about 13.65 times and 5.05 times higher than that of the ordinary ASI-G group. In vivo, the pharmacokinetics studies showed that ASI-NEs and ASI-NBGs reached the peak value in the skin quickly and maintained stable release for a long time with high bioavailability. ASI-NEs and ASI-NBGs were proved to be safe when applied for topical skin usage, and they could play a therapeutic role through the skin mainly by acting on the microstructure of the SC and by means of the skin adnexal pathways.

Conclusion: ASI-NEs and ASI-NBGs were effectively developed to overcome the barrier properties of the skin and show high drug penetration through the transdermal route. In addition, we found that ASI-NEs and ASI-NBGs are safe when applied through transdermal delivery system.

Keywords: asiaticoside, transdermal delivery system, permeation enhancer, nanoemulsions

Plain Language Summary

In clinical practice or treatment, asiaticoside is mainly used to treat a variety of skin diseases through transdermal delivery system, such as skin ulcer, keloid and scleroderma through transdermal delivery system, etc. However, the molecular weight of ASI is 911.1233 g/mol with low water solubility and poor lipophilicity, which limits the transdermal absorption tremendously. In this study, we designed asiaticoside-loaded nanoemulsions (ASI-NEs) and nanoemulsions-based gels (ASI-NBGs) and studied their mechanism for transdermal delivery. ASI-NEs and ASI-NBGs, particle size of 132±5.84 nm and solubility of 13.97 $mg \cdot g^{-1}$,

Correspondence: Li Zhang; Xiaohui Wang
Department of Pharmacy, Logistics College of Chinese People's Armed Police Forces, Tianjin 300309, People's Republic of China
Tel +86-13302086775; +86-13302023963
Email zhli62tianjin@163.com; 1517183319@qq.com

submit your manuscript | www.dovepress.com
DovePress
http://doi.org/10.2147/IJN.S241923

attenuate the barrier function of the stratum corneum, allowing ASI to transit into the underlying epidermis. The ASI permeability ratio (Qn) of the optimized ASI-NEs and ASI-NBGs are about 13.65 times and 5.05 times higher than that of the ordinary ASI-G group. Besides, ASI-NEs and ASI-NBGs are proved to be safe when applied for topical skin usage, and it appears that ASI-NEs and ASI-NBGs can play a therapeutic role through the skin mainly by acting on the microstructure of SC and by means of the skin adnexal pathways. The enhanced levels of ASI permeability ratio provide efficient and effective therapy for clinical application.

Introduction

Asiaticoside (ASI) is a triterpenoid extracted from Centella asiatica (L.) Urban[1] Studies have shown that ASI has the effects of promoting wound healing,[2] inhibiting the formation of skin scar,[3] anti-tumor,[4] anti-fibrosis,[5] neuroprotection,[6] antioxidant,[7] anti-depression,[8] anti-inflammation,[9] and lung protection.[10] At present, it is mainly used in clinical treatment of a variety of skin diseases, such as skin ulcer, keloid and scleroderma. And a large number of clinical practices have proved that topical ASI has a definite effect on human hypertrophic scar.[3] However, ASI has a molecular weight of 911.1233 g/mol, low water solubility and poor lipophilicity, which limit the transdermal absorption tremendously.[11]

The transdermal drug delivery system (TDDS) is attractive for the delivery of drugs in the treatment of a wide variety of diseases. As a route of drug application, TDDS has many advantages including good drug compliance, ease of application, continuous drug release, no hepatic first-pass effect, and lower organ toxicity for some drugs used chronically.[12] However, the transdermal process is mainly limited by the barrier properties of the skin's outer stratum corneum (SC),[13] and researches have shown that permeation enhancers,[14] microneedle,[15] therapeutic 1 MHz frequency sonophoresis,[16] nanocarriers,[17] iontophoresis[18] could contribute to overcome SC of the skin. Nanocarriers including transferosomes, liposomes, lipid nanoparticles, vesicles, polymer micelles and nanoemulsions (NEs) are widely used in TDDS. NEs, a carrier for transdermal administration, generally comprise appropriate proportions of oil, surfactant, cosurfactant, and water, which have advantages for drug delivery such as increasing drug solubility, improving skin affinity, reducing skin barrier effect and promoting drug permeability. The transdermal mechanism of NEs mainly includes strengthening the solubility of the drug, disordering the lipid bilayer of the SC, and increasing the hydration of the SC.[19] Besides, NEs can be prepared into nanoemulsion-based gels (NBGs) to reduce the mobility of NEs, prolong the retention time of NEs in skin, increase drug stability and improve the percutaneous absorption rate.[20]

In this study, asiaticoside-loaded nanoemulsions (ASI-NEs) and nanoemulsions-based gels (ASI-NBGs) were developed after selecting oils, surfactants, and cosurfactants. Using simplex lattice design (SLD), we determined the most suitable ratio of components to create an optimized formulation and demonstrated the mechanism of skin penetration in the application of ASI-NEs and ASI-NBGs. In addition, we investigated the skin irritation and skin pharmacokinetics of ASI-NEs and ASI-NBGs, so as to provide reference for the further development and application of new transdermal delivery systems.

Materials and Methods

Animals

All animal protocols complied with the Guide for the Care and Use of Laboratory Animals and Institute of Laboratory Animal Resources.

All the experiments on animals were approved by the Animal Ethics Committee of Logistics College of Chinese People's Armed Police Forces of Medical Sciences and performed in full compliance with international practices for animal care and use. Adult KM mice (18–22 g), Wistar rats (280–330 g), New Zealand white rabbit (2–3 kg) were obtained from the Laboratory Animal Center of Military Medical Science, PLA Academy, Beijing, China (License No. SCXK (Army)-2012-0004). All animals were housed in an environmentally (t=25±1°C) and air humidity (60%) controlled room with a 12 h light-dark cycle (light: 7:00 am to 7:00 pm). All animals were provided with a normal diet and water.

Materials

ASI (purity 98%) was obtained from Chengdu manster biotechnology Co., Ltd. (Chengdu, People's Republic of China). ASI (purity 60%) was obtained from Guangxichang natural pharmaceutical Co., Ltd. (Guangxi, People's Republic of China). Isopropyl palmitate (IPP) was obtained from Shanghai McLean biochemical technology Co., Ltd. (Shanghai, People's Republic of China). Glycerol monooleate was purchased from Liaoning kehai food chemical engineering Co., Ltd. (Liaoning, People's Republic of China). Glyceryl octyl decanoate (GTCC) was supplied by Qingdao yusuo chemical technology Co., Ltd. (Qingdao, People's

Republic of China). Ethoxylated hydrogenated castor oil (RH-40) was purchased from German BASF. Isopropyl myristate (IPM) was obtained from Sinopharm group chemical reagent Co., Ltd. (People's Republic of China). Castor oil, Polysorbate 20 (Tween 20), Polysorbate 80 (Tween 80), Polyethylene glycol 400 (PEG 400) were supplied by Tianjin fucheng chemical reagent factory (Tianjin, People's Republic of China). Oleic acid (OA), glycerol, and n-propanol were obtained from Tianjin first chemical reagent factory (Tianjin, People's Republic of China). 1,2-propanediol (PG) was purchased from Tianjin chemical reagent Co., Ltd. (Tianjin, People's Republic of China). Labrasol, Labrafac Lipophile WL 1349 (LL-WL1349), Plurol isostearique, Transcutol P and Plurol oleique were obtained from Gattefosse France (Gattefosse, France). Optimal Cutting Temperature Compound (OCT) (SAKURA, America). Fluorescein Isothiocyanate (FITC) was purchased from Everbright company (Everbright, America).

HPLC Analysis

ASI quantitative determinations were performed by using the LC-20AT High-Performance Liquid Chromatography (HPLC) (SHIMADZU, Japan) system with a reverse-phase Diamonsil® Plus 5C18-MS-II column (150×4.6 mm, 5μm). The mobile phase consisted of acetonitrile and pure water (25.5:74.5, v/v) at a flow rate of 0.8 mL/min. The column temperature was maintained at 30°C and the effluent was monitored at 220 nm. Quantified samples were filtered through a 0.22-μm filter membrane prior to automatic injection into the HPLC system.

Preparation of ASI-NEs

Screening of NEs Ingredients

To achieve maximized drug loading of ASI-NEs, the oils, surfactants and cosurfactants were selected on the basis of their ability to provide good solubilization for ASI. Excessive bulk ASI were added to 7 different oils, 4 surfactants and 8 cosurfactants. Then, the samples were treated by water bath shaking at 37°C for 24 h and centrifuged at 8000 r.min^{-1} for 20 mins. Finally, the supernatant was filtered through a membrane filter (0.22 μm), and the ASI saturation solubilities in oils, surfactants, cosurfactants were measured by HPLC, respectively.

Establishing of Pseudo-Ternary Phase Diagrams

All components were weighted and mixed under magnetic stirring by using the aqueous titration method at 37°C. It was crucial that the surfactants and cosurfactants are well proportioned for the development of NEs, which could affect the oil-water interfacial tension of the NEs.[21] A pseudo-ternary phase diagram was used to screen the ratio of surfactant to co-surfactant (K_m) for ASI-NE system.[22] Briefly, mixtures of surfactants and co-surfactants (S_{mix}) with different weight ratios (K_m=3:1, 2:1, 1:1, 1:2, respectively) were mixed with the selected oil phase at different weight ratios of 1:9, 2:8, 3:7, 4:6, 5:5, 6:4, 7:3, 8:2 and 9:1. Each combination was titrated slowly with distilled water under magnetic stirring at 600 r·min^{-1} until the solution became clear. Pseudo-ternary phase diagrams were constructed according to the ratios of oil, S_{mix} and distilled water.

Simplex Lattice Design Optimized Formulation of ASI-NEs

Then, SLD in design-expert 8.06 software was used to optimize the formulation. The NEs were composed of four phases and the total amount of oil phase, surfactant, cosurfactant and water was set at 100%. According to the region of NEs in the pseudo-ternary phase diagram, the content of each phase in the prescription was determined to be oil: 5%, Surfactant (X1): 15%~30%, Cosurfactant (X2): 15%–30%, Water (X3): 50%–65%. The contents of surfactant, cosurfactant and water were taken as independent variables, and solubility (Y1) and encapsulation efficiency EE (%) (Y2) were taken as evaluation responses. This scheme produced 14 experimental points, which were characterized by the Y1 and Y2. Then, the optimal ASI-NEs were gelled with 1% Carbomer 940 (BASF, German) to be ASI-NBGs.

Physical and Chemical Properties of ASI-NEs

Particle Size and PDI

Mean particle size and PDI were determined by BT-90 nanometer laser particle size distributor (Dandong, China).

pH Value

The pH value of ASI-NEs was determined by PHS-3C pH meter (Shanghai, China) at room temperature.

Encapsulation Efficiency

The free drug was separated from the drug encapsulated in the ASI-NEs by semipermeable membranes. PBS (pH=7.4) solution containing 0.6% RH40 was prepared as the dialysis medium and a dialysis membrane with a molecular interception of 3000 (Union Carbide, America) were placed in the dialysis medium for pre-boiling for 1 h for activation. The precise amount of ASI-NEs 4 mL was

taken in dialysis membrane, clamped at both ends, placed in 200 mL dialysis medium, stirred at 37°C, 130 r·min^{-1} for 4 h. Then, the dialysis medium was taken 1 mL out, filtered with 0.22-μm microporous membrane, and measured by HPLC to determine the concentration of free drugs. The total and separated drug contents were measured by HPLC, and the EE (%) was mathematically calculated according to Equation 1:

$$EE\% = \frac{1 - C_{free}}{C_{total}} \times 100\% \quad (1)$$

Stability of ASI-NEs

The stability of ASI-NEs was determined by high-speed centrifugation method. A volume of 5 mL of ASI-NEs sample was centrifuged in a 10 mL centrifugal filter tube by SIGMA 1–14 small table centrifuge (German) at 12,000 r·min^{-1} for 15 min to observe the appearance and stratification.

Each measurement was carried out in triplicate and standard deviations were calculated.

Evaluation of Transdermal Permeation in vitro

We used the RYJ-6B Franz diffusion cell (Shanghai, China) to conduct in vitro transdermal experiments with the volume of receiving pool V (15 mL) and contact area A (2.8 cm^2). Seven groups were prepared in vitro transdermal test.

The hair on the abdominal area of rats was removed at the day before the experiment,[23] 20% ethanol phosphate buffer saline solution (PBS) was used as the receiver solution. The skins of SD, as the percutaneous medium, were tightly fixed on the diffusion pool. The receiver solution and its watery environment were completely adjusted to the constant temperature at 37±1°C, and electromagnetically stirred at a constant speed of 150 r/min. All the receiving solution was collected at 0.5 h, 1 h, 2 h, 4 h, 6 h, 8 h, and 12 h, respectively, for each group, and new liquid was added at the same time. Then, drug concentrations (C_i, μg/mL) of each sample were analyzed by HPLC described above, and the cumulative penetration amount per unit area at all time points (Q_A, μg/cm^2) was calculated as shown in Equation 2:

$$Q_A = \frac{V(C_n + \sum_{i=1}^{n-1} C_i)}{A} \quad (2)$$

Skin Pharmacokinetics

A total of 120 mice were chosen and randomly divided into 3 groups: the commercially ASI gels group, the ASI-NEs group, the ASI-NBGs group. The back hair of the mice was shaved 12 h before the experiment. In addition, a work area of 4 cm^2 was selected to administer drugs with dosages of 0.60 g/mouse each group. Then, the residual drug on back was removed at 0.5 h, 1 h, 2 h, 4 h, 6 h, 8 h and 12 h, and the mice were dislocated neck to dead. The skin of drug area was peeled off and washed three times with normal saline, blotted with filter paper, and weighed precisely. Then, the skin was put into 10 mL centrifuge tube with 5 mL methanol, whirled 2 min and vibrated in water at 37 ±1°C for 24 h. Finally, the SB-5200DTN ultrasound cleaner (Ningbo, China) was used for 4 times, each time for 30 min, to fully extract ASI from the skin. And the liquid was measured using HPLC to study the skin pharmacokinetics.

Evaluation of Skin Irritation

Using the skin of New Zealand white rabbit, the irritation potential of ASI-NEs and ASI-NBGs was studied. Animals were allocated into two groups (1st group-normal skin group (Figure 1A), 2nd group-damage group (Figure 1B)) having six animals (n=6) in every group.[24] The model of damage skin in rabbit was scratched slightly with a sterilized surgical scalpel, which was advisable to have a little exudative blood in the skin. There were two methods of administration: single administration and multiple administration.

Single administration: normal skin and damaged skin were given 0.6 g of each medicine in the designated area, and the tested area was washed with warm water 24 h later to remove residual drugs. The presence of erythema and edema on the medication site was observed and recorded at 1 h, 24 h, 48 h and 72 h after removing residual drugs, scored according to skin irritation criteria (Table 1), evaluated the stimulation intensity.

Multiple administration: the dose was the same as the single dose, and the dose frequency was once a day for 7 days. The presence of erythema and edema on the medication site was observed every day, recorded 1 h, 24 h, 48 h and 72 h after the last time of administration of the drug, scored according to skin irritation criteria (Table 1), evaluated the stimulation intensity.

The system includes two irritation signs (erythema/redness, and edema/swelling) and their severity shown in Table 2. The average skin irritation score (M) was calculated according to Equation 3. The skin irritation strength was evaluated as the criteria (no irritation, M=0–0.49; mild irritation, M=0.5–2.99; moderate irritation, M=3.0–5.99; severe irritation, M=6.0–8.0).

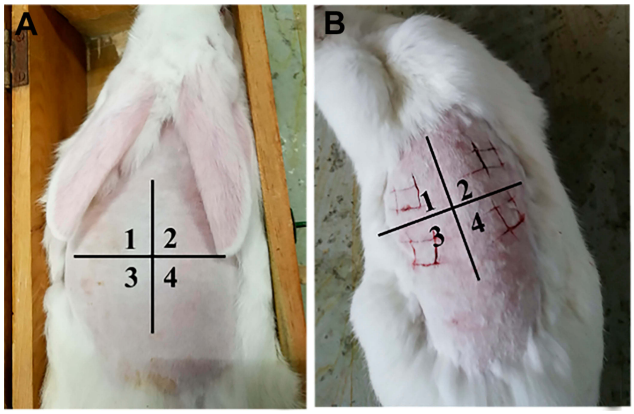

Figure 1 The area of various preparations on rabbits.
Notes: Dorsal hair of each rabbit was shaved and divided into four zones: the normal saline (zone 2, zone 3), ASI-NEs (zone 1) and ASI-NBGs (zone 4), respectively, and each zone was about 4 cm^2. Animals were allocated into two groups: damage skin group (**A**); normal group (**B**).
Abbreviations: ASI-NEs, asiaticoside-loaded nanoemulsions; ASI-NBGs, asiaticoside-loaded nanoemulsions-based gels.

$$M = \frac{\text{erythema total scores} + \text{edema total scores}}{6} \quad (3)$$

HE Stained

The skin of the rabbit, given the multiple administration of drug in normal groups under item "evaluation of skin irritation", was peeled off about 1 cm^2 each zone, washed with warm water, blotted by filter paper, buried with OCT, and stored at −80°C. The temperature of the freezing microtome was adjusted to −21°C at 30 min before slicing. The embedded skin mass was cut longitudinally, from the subcutaneous tissue layer to the epidermis. And 6 μm longitudinal sections of the OCT-embedded skin were obtained, which were blew to be dry, conducted regular HE stained, and sealed the slices with neutral gum. The prepared sections were examined under an upright metallurgical microscope (Olympus, Japan).[25]

Table 1 The Standard of Skin Irritation Response

	Present	Score
Erythema	None present	0
	Mild erythema	1
	Moderate erythema	2
	Severe erythema	3
	Purplish red erythema with focal anthemia	4
Edema	None present	0
	Mild edema	1
	Moderate edema	2
	Severe edema	3
	Severe edema (edema swelling over 1mm)	4
Total scores		8

Confocal Laser Scanning Microscopy (in vivo Optical Imaging Study)

Fluorescein Isothiocyanate (FITC) was accurately weighed and 0.5 mM FITC solution (FITC-s) was prepared as the control group. According to the preparation method of NEs, FITC and ASI bulk drug were added at the same time as the internal phase to prepare FITC-ASI-NEs and FITC-ASI- NBGs containing 0.5 mM FITC.[26] The prepared fluorescent-labeled samples were wrapped in tin foil and stored in a 4°C refrigerator.

Forty-five mice were chosen and randomly divided into 3 groups, and the back hair of the mice was shaved about 4 cm^2 12 h before the experiment. To visualized the permeation, 0.5 h, 2 h, 6 h in vivo pretreated hairless mice with 0.6 g FITC-ASI-NEs, FITC-s, and FITC-ASI- NBGs was sacrificed, respectively. 6 μm longitudinal sections of the OCT-embedded skin were examined under TSC-SP8 Confocal laser scanning microscopy (CLSM). (Leica, Germany), the light source Ar/He/Ne, the excitation wavelengths of fluorescence probes DAPI and FITC were 360 nm and 488 nm, respectively, and the pinhole size was fixed. When CLSM observed the fluorescence of DAPI and FITC, the gray values were set at 625 and 647, respectively. Images were collected, and image-pro plus 6.0 software was used to calculate the fluorescence area and integrated optical density (IOD) of the image, which was used as the evaluation index of drug penetration, retention and distribution in the skin.

Statistical Analysis

All results were analyzed and are expressed as the mean ± SD. Differences between groups were assessed via the analysis of variance and the independent samples test using the SPSS software package (SAS Institute, Cary, NC, USA), and $P<0.05$ was considered statistically significant.

Results and Discussion

Preparation of ASI-NEs

Solubility

The transdermal permeation of ASI has generally been limited by its poor water solubility. Therefore, selecting the suitable components to obtain maximum solubilization of ASI was a vital step for the preparation of ASI-NEs, especially for the development of TDDS. The results of the drug solubility tests

Table 2 Experimental Design and Results (SLD)

Formulation	X_1 Surfactant	X_2 Cosurfactant	X_3 Water	Y_1 Solubility (mg·g^{-1})	Y_2 EE (%)
1	0.30	0.15	0.50	11.55	94.87
2	0.15	0.3	0.50	15.05	72.59
3	0.15	0.15	0.65	9.05	84.05
4	0.225	0.225	0.50	12.43	57.55
5	0.225	0.15	0.575	8.99	89.32
6	0.15	0.225	0.575	14.6	92.32
7	0.25	0.175	0.525	9.66	63.95
8	0.175	0.25	0.525	14.99	91.48
9	0.175	0.175	0.6	10.72	94.89
10	0.20	0.20	0.55	13.13	82.38
11	0.30	0.15	0.50	11.64	92.19
12	0.15	0.30	0.50	16.48	78.25
13	0.15	0.15	0.65	9.39	70.06
14	0.225	0.225	0.5	14.17	63.14

Abbreviation: EE, encapsulation efficiency.

in various oils (A), surfactants (B) and cosurfactants (C) are shown in Figure 2A–C, which indicated that ASI had the maximum drug solubilities in Glycerol monooleate (oil) (1742.98±19.35 μg/g), RH-40 (surfactant) (4785.87±28.92 μg/g) and Transcutol P (cosurfactant) (67,492.31±977.89 μg/g). Glycerol monooleate is a compound with low solubility in water, high melting point, and high toxicity. However, nanostructuration could significantly decrease the toxic effects of Glycerol monooleate.[27] ASI had the highest solubility in RH-40 compared with that of other surfactants. Transcutol P has the maximum solubilization for ASI and was considered the appropriate cosurfactant for preparing the ASI-NEs. In addition, Transcutol P exhibits the characteristics of exceptionally low skin irritation, excellent solubilization ability and great permeability.[28] Conclusively, glycerol monooleate, RH-40, and Transcutol P were selected as the best oil, surfactant and co-surfactant compositions, respectively.

Pseudo-Ternary Phase Diagrams

S_{mix} with optimal ratio showed the advantage of increasing the stability of NEs, enlarging the emulsification region of NEs, and reducing the irritation of NEs.[29,30] In this report, the S_{mix} ratios used to form the NEs were screened with pseudo-ternary phase diagrams. The numeric value of emulsifying regions in the pseudo-ternary phase diagram was quantized using Origin® (2017). According to the calculation results and data in Figure 3 A–D, the ASI-NEs with a K_m ratio of 1:1 (B) and 1:2 (A) showed larger emulsifying region compared to that of the ratios of 2:1 (C) and 3:1 (D), which indicated the ASI-NEs could be more easily spontaneously emulsify and have better stability at a K_m ratio of 1:1–1:2. Thus, the most appropriate ratio of K_m to prepare the ASI-NEs between 1:1–1:2 needed to be optimized further.

Simplex Lattice Design Optimized Formulation of ASI-NEs

The SLD method was used to screen the final ASI-NE formulation with the desired properties for further experiments. Response data for all experiments are given in Table 2. The multiple regression model was fitted with the design-expert 8.06 software, and the response equation of two responses was obtained, respectively:

Y1=10.37826X1+47.20493 X2+1.19967X3 (R^2=0.8328, P<0.0001, $P_{lack\ of\ fit}$ =0.2019)

Y2=7.97770 X1-9.83820 X2-3.38111X3-42.44365 X1X2+4.67780X1X3+ 38.51526 X2X3 (R^2= 0.7019, P=0.0474, $P_{\text{lack of fit}}$ =0.1084)

The coefficients R^2 of the two fitted regression equations were both high, which indicated that the fitting degrees were good. P values of the fitted regression equation were both <0.05, suggesting that the response regression model reached a significant level. The P values of lack of fit were both >0.05, indicating that the relevance to the pure error was not significant. Conclusively, the fitted regression equations of the two responses were successful. According to the fitting equation Y1, the proportion of cosurfactant had a great influence on the solubility of the ASI in ASI-NEs. As for the fitting equation Y2, surfactant, cosurfactant and water all played a great role on EE (%). Figure 4A and B shows contour diagram of solubility (A), and contour diagram of EE (%) (B).

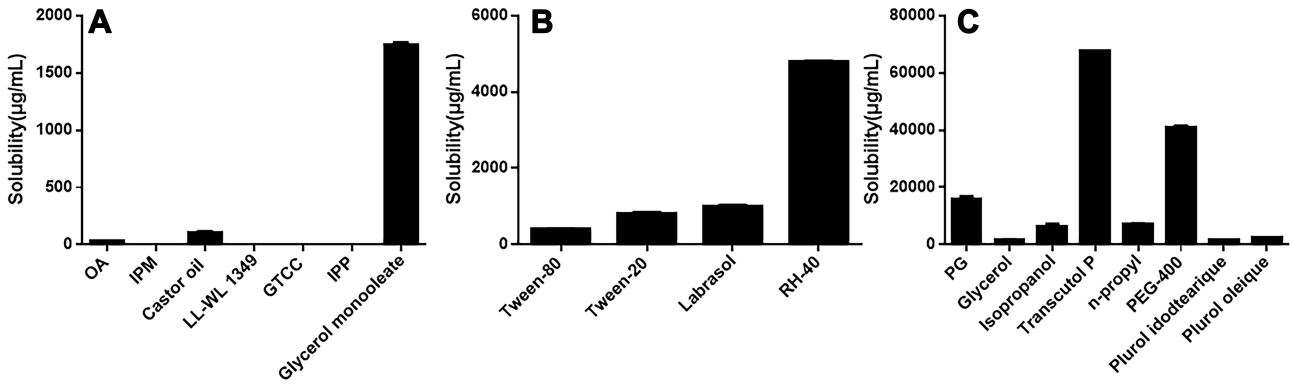

Figure 2 Solubility of ASI in different oils (**A**), surfactants (**B**) and cosurfactants (**C**).

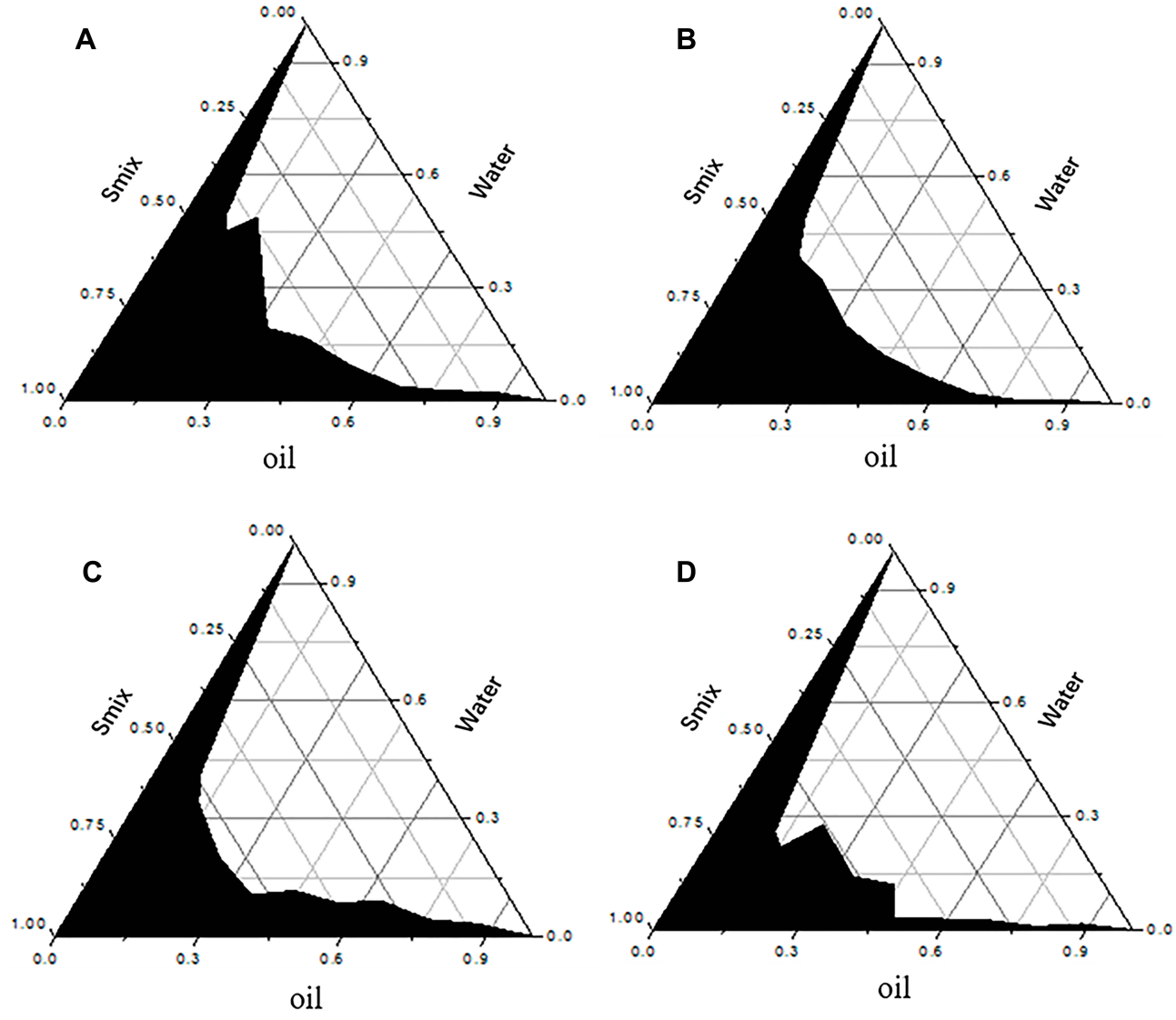

Figure 3 Pseudo-ternary phase diagrams of glycerol monooleate/RH-40/Transcutol P/water system.
Notes: K_m=1:2 (**A**), K_m=1:1 (**B**), K_m=2:1 (**C**), and K_m=3:1(**D**).
Abbreviation: RH-40, ethoxylated hydrogenated castor oil.

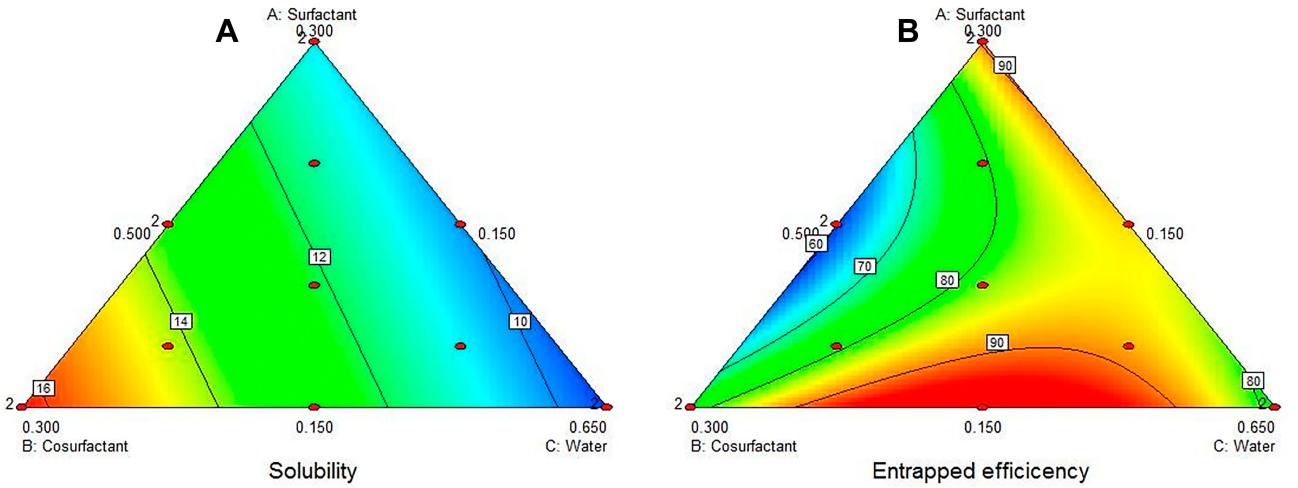

Figure 4 Contour plots of solubility (**A**) and EE (%) (**B**).
Abbreviation: EE, encapsulation efficiency.

According to the two fitting equations, two theoretical optimal prescriptions can be obtained, as shown in Table 3.

Then, three batches of NEs were prepared, respectively, according to the two theoretical optimal prescriptions, and the predicted optimum ranges of the independent variables (Table 4) showed that the experimental values were very close to the predicted values with low percentage bias, suggesting that the optimized formulation was reliable and reasonable. The proportion of mixed surfactants in prescription 1 and prescription 2 was 41.3% and 45%, respectively. Precious research has shown that the skin irritation increased with the amount of mixed surfactant.[28] Therefore, prescription 1 was selected as the optimal prescription for ASI-NEs preparation ultimately. The prepared optimal ASI-NBGs was colorless, clear, transparent, without caking, and stable in appearance.

Characterization of ASI-NEs

Particle size is a vital standard to authenticate the NEs.[31] Particle size and PDI of the optimized formulation are shown in Figure 5. ASI-NEs were nanometric and unimodal with a relatively narrow size distribution (PDI=0.2211) and an average diameter of 132±5.84 nm. The results showed that ASI-NEs was uniform in particle size and concentrated in distribution. The pH of ASI-NEs was 6.8, which was safe and could be used for transdermal delivery system directly. High-speed centrifugation results showed that no stratification, turbidity or precipitation occurred after ASI-NEs centrifugation, indicating that ASI-NEs was relatively stable.

Evaluation of Transdermal Permeation in vitro

In this study, the in vitro transdermal permeation of seven different ASI formulations was studied for 12 h. The cumulative release curve is shown in Figure 6. The results showed that the percutaneous penetration of ASI in vitro was in line with the zero-order dynamic model, and the cumulative penetration per unit area (Q) was in a good linear relationship with time. Results indicated that, comparing with the ordinary ASI-Gel, the three transdermal enhancer groups, which contained transdermal absorption stimulant: 5% borneol, 5% menthol and 5% azone, showed better permeability ratio with 1.30 times, 1.49 times and 1.04 times, respectively. Furthermore, ASI-NEs and ASI-NBGs significantly increased the ASI permeability ratio by 13.65 times and 5.05 times, respectively, compared with the ordinary ASI-Gel ($P < 0.01$, $P < 0.01$).

Table 3 The Theoretical Optimal Prescription (SLD)

Formulation	X_1 Surfactant	X_2 Cosurfactant	X_3 Water	Y_1 Solubility (mg g^{-1})	Y_2 EE (%)	Desirability
1	0.150	0.263	0.537	14.605	93.620	0.851
2	0.300	0.150	0.500	10.794	90.737	0.463

Abbreviation: EE, encapsulation efficiency.

Table 4 Comparison of Predicted and Experimental Values of ASI-NEs (n=3)

Formulation	Solubility (mg g^{-1}) Predicted	Experimental	Bias%	EE (%) Predicted	Experimental	Bias%
1	14.6048	13.9689±0.3155	4.55	93.6203	90.2861±0.0268	3.69
2	10.7941	10.1397±0.0304	6.45	90.7373	86.2995±0.3921	5.14

Note: Bias (%) = (predicted values - experimental values)/experimental values×100.
Abbreviations: EE, encapsulation efficiency; ASI-NEs, asiaticoside-loaded nanoemulsions.

Evaluation of Skin Irritation

ASI-NEs and ASI-NBGs skin irritation test showed no irritation to normal skin and damaged skin after single administration, and the evaluation of stimulation intensity is shown in Table 5. After multiple administration, ASI–NBGs had no irritation to the normal skin, while ASI-NEs has mild irritation, as shown in Table 6. ASI-NBGs had less skin irritation than ASI-NEs, which might be due to the fact that the three-dimensional structure of the gel formed by carbomer 940 avoided the direct contact between the skin and ASI-NEs. The results indicated that ASI-NBGs was a safe topical preparation for skin, but should not be used on damaged skin.

Skin Pharmacokinetics

According to ASI concentration of each group, the skin pharmacodynamic parameters are shown in Table 7. The results indicated that ASI–NEs and ASI–NBGs peeked faster, released stably in longer term, kept the quality of drug concentrations in the subcutaneous tissue in a relatively constant level, had higher bioavailability, and had a facilitating effect on ASI transdermal absorption.

HE Stained

Microscopically, HE stained showed that the skin structure of the control group (Figure 7A) was complete, with layers of epidermis arranged closely, neatly, and clear stratification. The keratin cells were closely connected, and fewer keratin fragments could be observed. After using ASI-NEs (Figure 7B) and ASI-NBGs (Figure 7C), the SC was loose and thin, the keratin fragment increased, the intercellular space in the spinous layer increased, and the basal layer cells were loosely arranged. The results showed that the permeability enhancement of ASI-NEs and ASI-NBGs was related to the change of skin microstructure. NEs, as a transdermal drug delivery carrier, can thin out the dense membrane structure formed by lipids, proteins and non-fibrin, weaken its barrier effect. This will provide a reference for the further study of NEs as transdermal drug delivery carrier.

Confocal Laser Scanning Microscopy (in vivo Optical Imaging Study)

ASI-NEs and ASI-NBGs were labeled with FITC fluorescent probe to study the transdermal mechanism FITC-ASI-NEs and FITC-ASI-NBGs. The fluorescence of each formulation

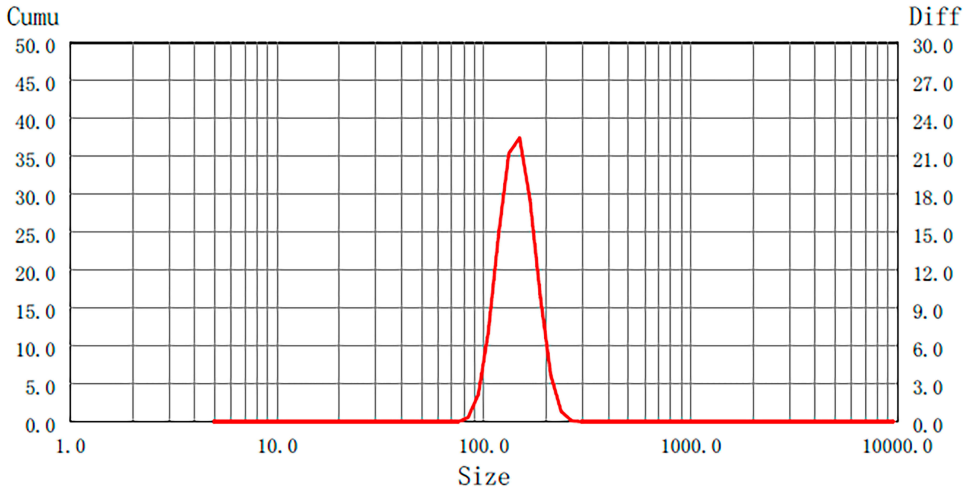

Figure 5 Average particle size and distribution of ASI-NEs.
Abbreviation: ASI-NEs, asiaticoside-loaded nanoemulsions.

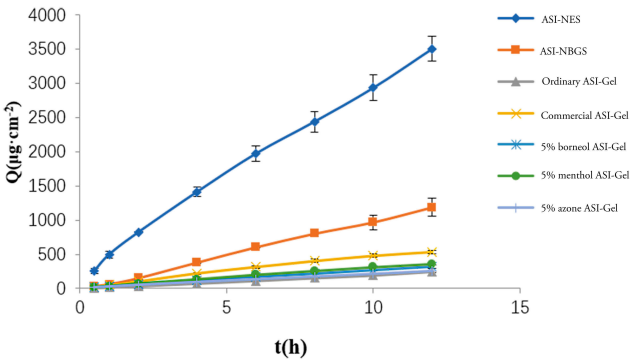

Figure 6 The accumulative percutaneous absorption quantity curves of ASI (n=3).
Notes: The commercially ASI-Gel group, the ordinary ASI-Gel group, the 5% azone ASI-Gel group, the 5% menthol ASI-Gel group, the 5% borneol ASI-Gel group, the ASI-NEs group and the ASI-NBGs group. The transdermal formulations were applied for 12 h.
Abbreviations: ASI, asiaticoside; ASI-NEs, asiaticoside-loaded nanoemulsions; ASI-NBGs, asiaticoside-loaded nanoemulsions-based gels.

at different time points is shown in Figure 8. FITC-S penetrated slowly, stored only in the cuticle within 2 h, and penetrated into the dermis within 6 h (Figure 8A). FITC-ASI-NEs penetrated into the dermis at 30 min and was evenly distributed in the dermis at 6 h (Figure 8B). The IOD and fluorescence area of skin sections were 28.81 times and 32.51 times of that of the FITC-S group, respectively (Tables 8 and 9). FITC-ASI-NBGs permeated rapidly, and fluorescence was observed in the dermis at 30 min with increasing intensity (Figure 8C). IOD and fluorescence area at 6 h were 2.06 times and 2.28 times of the FITC-S group, respectively (Tables 8 and 9). It illustrated that FITC-ASI-NEs and FITC-ASI-NBGs had strong percutaneous penetration, fast transdermal penetration and high drug retention, which were distributed in the corneum, dermis, sweat gland adjunct and other parts. CLSM results also showed that sweat glands, hair follicles and other skin appendices also provided effective pathways for ASI-NEs and ASI-NBGs transdermal penetration.

Table 5 Average Response Scores of Skin Irritation for Single Applications (n=6)

Group	Preparations	Average Scores			
		1h	24h	48h	72h
Normal skin	Control	0	0	0	0
	ASI-NEs	0	0	0	0
	ASI-NBGs	0	0	0	0
Damaged skin	Control	0	0	0	0
	ASI-NEs	0.40	0	0	0
	ASI-NBGs	0.20	0	0	0

Note: Control: the normal saline.
Abbreviations: ASI-NEs, asiaticoside-loaded nanoemulsions; ASI-NBGs, asiaticoside-loaded nanoemulsions-based gels.

Table 6 Average Response Scores of Skin Irritation for Multiple Applications (n=6)

Group	Preparations	Average Scores			
		1h	24h	48h	72h
Normal skin	Control	0	0	0	0
	ASI-NEs	0.60	0.20	0	0
	ASI-NBGs	0.40	0	0	0
Damaged skin	Control	0	0	0	0
	ASI-NEs	0.60	0.20	0	0
	ASI-NBGs	0.60	0.20	0	0

Note: Control: normal saline.
Abbreviations: ASI-NEs, asiaticoside-loaded nanoemulsions; ASI-NBGs, asiaticoside-loaded nanoemulsions-based gels.

Table 7 Pharmacokinetic Parameters in Skin After the Application Administration of ASI Transdermal Delivery Systems

Parameter	ASI-Gel	ASI-NEs	ASI-NBGs
t_{max}/h	8	6	6
C_{max}/μg g^{-1}	203.81±10.07	656.28±19.42**	493.17±36.71**
AUC $_{0\text{-}12h}$/ μg·h g^{-1}	1613.91 ±35.42	3615.55±75.47**	3184.40±52.65**
AUC $_{0\text{-}\infty}$/μg·h g^{-1}	2321.36 ±93.14	6227.85 ±169.43**	4994.90 ±101.39**

Notes: **vs the ordinary ASI-Gel, P<0.01.
Abbreviations: ASI-NEs, asiaticoside-loaded nanoemulsions; ASI-NBGs, asiaticoside-loaded nanoemulsions-based gels.

Discussion

The results showed that the transdermal rate and skin retention of the seven preparations from the largest to the smallest were ASI-NEs, ASI-NBGs, the 5% menthol ASI-Gel, the 5% borneol ASI-Gel and the 5% azone ASI-Gel, successively. Menthol is a terpene transdermal enhancer. Its main mechanism is to promote the diffusion of drug, break down the intercellular lipid barrier in the cuticle, improve tissue conductivity, open the polar channel in the cuticle, and increase drug distribution from matrix to cuticle.[32,33] Menthol preferentially distributes into the intercellular spaces of the SC, thus altering the barrier properties of the SC and causing a reversible disruption of the lipid domains, resulting in an increase in drug skin absorption.[34] To date, borneol has been reported as a permeation enhancer for both hydrophobic and hydrophilic drugs, especially the former. Recent studies have indicated that at high concentrations (>0.054%), borneol led to the

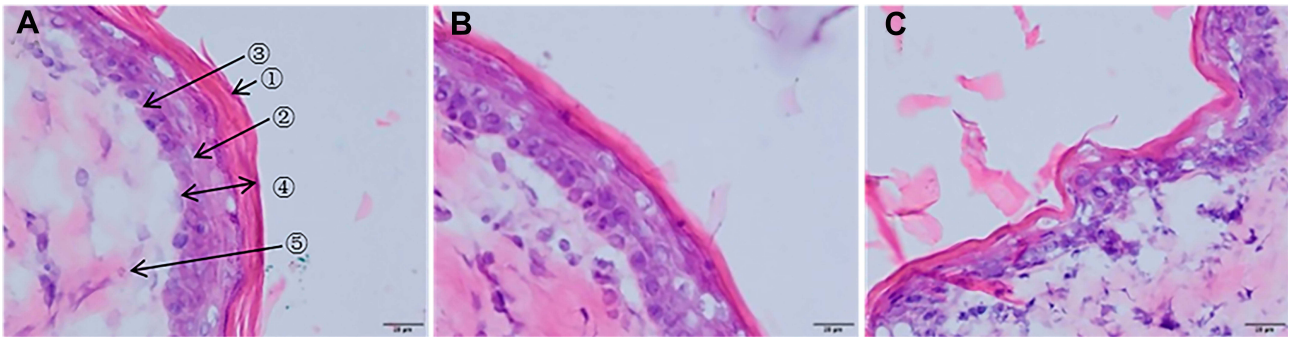

Figure 7 Histological photomicrographs of frozen section taken from rabbit treated with various applications (× 400).
Notes: Saline (**A**); ASI-NEs (**B**); ASI-NBGs (**C**); ①stratum corneum; ②stratum spinosum; ③ stratum basale; ④ epidermis; ⑤dermis.
Abbreviations: ASI-NEs, asiaticoside-loaded nanoemulsions; ASI-NBGs, asiaticoside-loaded nanoemulsions-based gels.

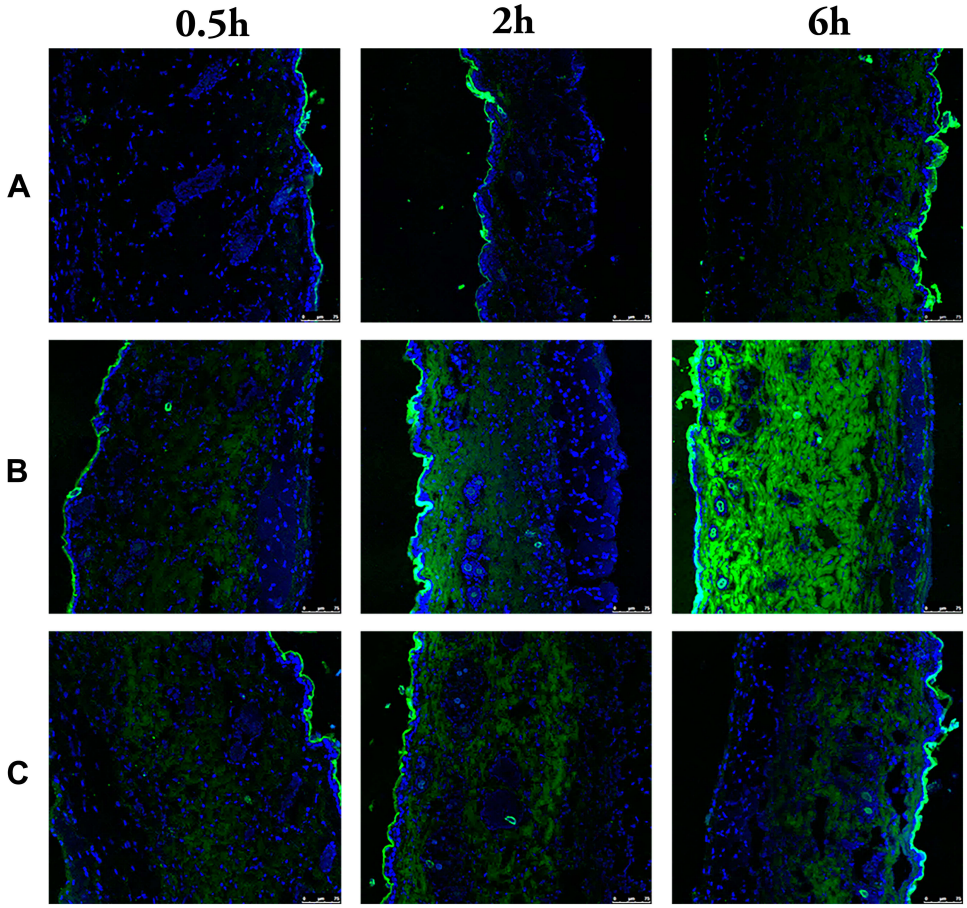

Figure 8 Laser scanning confocal micrograph of the mice skin treated with FITC-S (**A**), FITC-ASI-NEs (**B**) and FITC-ASI-NBGs (**C**) at 30 min, 2 h and 6 h.
Abbreviations: FITC-S, FITC aq. solution; FITC-ASI-NEs, FITC-asiaticoside-loaded nanoemulsions; FITC-ASI-NBGs, FITC-asiaticoside-loaded nanoemulsions-based gels.

formation of water pores and long-lived reversed micelles, which improved the permeation of osthole and possibly other hydrophobic or hydrophilic drugs through the SC. However, the permeation effect of borneol was inhibited at low concentration (0%–0.54%).[35] Azazone, also known as laurazine, is the first compound developed specifically for skin penetration enhancers, which increase skin transdermal absorption of different types of drugs. The main mechanism is to decrease the temperature of lipid phase transition, increase lipid fluidity, and thus increase drug penetration. NEs were selected as the ASI

Table 8 Fluorescence Area of FITC in Treated Skin (n=3)

Formulation		Area (10^3)/μm2	
	30 min	2 h	6 h
FITC-S	8.34±0.26	8.58±0.82	13.36±1.67
FITC-ASI -NEs	8.47±0.82	53.84±1.44**	384.92±7.60**
FITC- ASI -NBGs	8.41±0.61	14.39±1.12**	27.48±1.81**

Notes: **vs FITC aq. solution, $P<0.01$

Abbreviations: FITC, fluorescein isothiocyanate; FITC-S, FITC aq. solution; FITC-ASI-NEs, FITC-asiaticoside-loaded nanoemulsions; FITC-ASI-NBGs, FITC-asiaticoside-loaded nanoemulsions-based gels.

Table 9 Integrated Optical Density of FITC in Treated Skin (n=3)

Formulation		IOD (10^6)	
	30 min	2 h	6 h
FITC-S	1.62±0.07	1.58±0.10	2.42±0.27
FITC-ASI -NEs	1.92±0.16*	10.99±0.25**	78.67±0.55**
FITC- ASI -NBGs	1.64±0.12	2.85±0.22**	5.52±0.42**

Notes: *vs FITC aq. solution, $P<0.05$; **vs FITC aq. solution, $P<0.01$.

Abbreviations: FITC, fluorescein isothiocyanate; FITC-S, FITC aq. solution; FITC-ASI-NEs, FITC-asiaticoside-loaded nanoemulsions; FITC-ASI-NBGs, FITC-asiaticoside-loaded nanoemulsions-based gels; IOD, integrated optical density.

carrier in this study for the advantages of simple preparation, strong stability, high solubility, and improved drug penetration.[36] The transdermal mechanism of NEs mainly includes improving the solubility of the drug, increasing the hydration of the SC, disordering the lipid bilayer of the SC.[19,37] Previous researches have indicated that NEs with appropriate particle size, sufficient drug loading, positive surface charge could effectively promote the penetration into skin.[38]

SC has a name "brick wall structure", which is the main barrier of drug absorption through skin.[39] After removing the SC in SD rats, the percutaneous penetration of raloxifene nanoparticles was significantly improved comparing with that of skin with SC,[13] which indicated that skin epidermal structure has a strong inhibition effect on drug penetration. This study shows that ASI-NEs and ASI-NBGs have good transdermal performance. The transdermal mechanisms include mainly disrupting the microstructure of the SC, thinning the dense membrane structure formed by lipids, proteins, non-fibrin, and weakening its barrier effect. Besides, the skin adnexal pathway also takes an important role in transdermal absorption of NEs. However, many studies have prepared NEs on the basis of different components, and the specific components that caused the mechanism need to be further studied. We speculate that the mechanism of preparing NEs in this study is closely related to surfactant RH-40 and cosurfactant Transcutol P.

Conclusion

In this study, SLD was successfully used to optimize the composition of the ASI-NEs formulation. According to the ex vivo permeation study, the ASI-NEs exhibited significantly higher transdermal permeation than that of the enhancer groups. The nanoscale size and sufficient drug load of the ASI-NEs contributed to the transfer of ASI from the nanovehicle to the skin. Studies on mouse skin pharmacokinetics have shown that after local administration, the drug in ASI-NEs and ASI-NBGs reached the peak value in the skin quickly, maintained stable release for a long time and keep the drug mass concentration in the subcutaneous tissue at a relatively constant level with high bioavailability. In addition, the transcutaneous mechanism of ASI-NEs and ASI-NBGs, studied by HE stained and CLSM, showed that the drug can play a therapeutic role mainly by disrupting microstructure of the cuticle and by means of the skin adnexal pathways. As summarized above, the ASI-NBGs is a promising topically administered preparation for the treatment of skin scar in future clinical.

Acknowledgment

This work was supported by the basic research project of Logistics University of Chinese People's Armed Police Force.

Disclosure

Qian Peng is affiliated with Jiangsu Hengrui Pharmaceutical Co. LTD. The authors report no other conflicts of interest in this work.

References

1. Ozdemir O, Ozkan K, Hatipoglu F, et al. Effect of asiaticoside, collagenase, and alpha-chymotrypsin on wound healing in rabbits. *Wounds*. 2016;28(8):279–286.
2. Verma N, Kumari U, Mittal S, et al. Effect of asiaticoside on the healing of skin wounds in the carp Cirrhinus mrigala: an immunohistochemical investigation. *Tissue Cell*. 2017;49(6):734–745. doi:10.1016/j.tice.2017.10.005
3. Pan S, Li T, Li Y. [Effects of asiaticoside on cell proliferation and Smad signal pathway of hypertrophic scar fibroblasts]. *Zhongguo Xiu Fu Chong Jian Wai Ke Za Zhi*. 2004;18(4):291–294. Chinese.
4. Al-Saeedi FJ. Study of the cytotoxicity of asiaticoside on rats and tumour cells. *BMC Cancer*. 2014;25(14):220. doi:10.1186/1471-2407-14-220
5. Dong MS, Jung SH, Kim HJ, et al. Structure-related cytotoxicity and anti-hepatofibric effect of asiatic acid derivatives in rat hepatic stellate cell-line, HSC-T6. *Arch Pharm Res*. 2004;27(5):512–517. doi:10.1007/BF02980124
6. Chen S, Yin ZJ, Jiang C, et al. Asiaticoside attenuates memory impairment induced by transient cerebral ischemia-reperfusion in mice through anti-inflammatory mechanism. *Pharmacol Biochem Behav*. 2014;122:7–15. doi:10.1016/j.pbb.2014.03.004
7. Guo JS, Cheng CL, Koo MW. Inhibitory effects of centella asiatica water extract and asiaticoside on inducible nitric oxide synthase during gastric ulcer healing in rats. *Planta Med*. 2004;70(12):1150–1154. doi:10.1055/s-2004-835843

8. Luo L, Liu XL, Mu RH, et al. Hippocampal BDNF signaling restored with chronic asiaticoside treatment in depression-like mice. *Brain Res Bull*. 2015;114:62–69. doi:10.1016/j.brainresbull.2015.03.006
9. Yun KJ, Kim JY, Kim JB, et al. Inhibition of LPS-induced NO and PGE2 production by asiatic acid via NF-kappa B inactivation in RAW 264.7 macrophages: possible involvement of the IKK and MAPK pathways. *Int Immunopharmacol*. 2008;8(3):431–441. doi:10.1016/j.intimp.2007.11.003
10. Wang XB, Wang W, Zhu XC, et al. The potential of asiaticoside for TGF-β1/Smad signaling inhibition in prevention and progression of hypoxia-induced pulmonary hypertension. *Life Sci*. 2015;137:56–64. doi:10.1016/j.lfs.2015.07.016
11. Ren Y, He XD, Shang BC, et al. [Analysis on preparation and characterization of asiaticoside-loaded flexible nanoliposomes]. *Zhongguo Zhong Yao Za Zhi*. 2013;38(19):3282–3286. Chinese.
12. Subbiah N, Campagna J, Spilman P, et al. Deformable nanovesicles synthesized through an adaptable microfluidic platform for enhanced localized transdermal drug delivery. *J Drug Deliv*. 2017;2017:4759839. doi:10.1155/2017/4759839
13. Nagai N, Ogata F, Otake H, et al. Design of a transdermal formulation containing raloxifene nanoparticles for osteoporosis treatment. *Int J Nanomedicine*. 2018;13:5215–5229. doi:10.2147/IJN.S173216
14. Kim KT, Kim S, Kim MH, et al. Effect of enhancers on in vitro and in vivo skin permeation and deposition of S-Methyl-(L)-Methionine. *Biomol Ther (Seoul)*. 2017;25(4):434–440. doi:10.4062/biomolther.2016.254
15. Li J, Zeng M, Shan H, et al. Microneedle patches as drug and vaccine delivery platform. *Curr Med Chem*. 2017;24(22):2413–2422. doi:10.2174/0929867324666170526124053
16. Park D, Ryu H, Kim HS, et al. Sonophoresis using ultrasound contrast agents for transdermal drug delivery: an in vivo experimental study. *Ultrasound Med Biol*. 2012;38(4):642–650. doi:10.1016/j.ultrasmedbio.2011.12.015
17. Carita AC, Eloy JO, Chorilli M, et al. Recent advances and perspectives in liposomes for cutaneous drug delivery. *Curr Med Chem*. 2018;25(5):606–635. doi:10.2174/0929867324666171009120154
18. Giri TK, Chakrabarty S, Ghosh B. Transdermal reverse iontophoresis: a novel technique for therapeutic drug monitoring. *J Control Release*. 2017;246:30–38. doi:10.1016/j.jconrel.2016.12.007
19. Lane ME. Skin penetration enhancers. *Int J Pharm*. 2013;447(1–2):12–21. doi:10.1016/j.ijpharm.2013.02.040
20. Xiao YY, Liu F, Chen ZP, et al. [Microemulsion-based gel of fluorouracil for transdermal delivery]. *Yao Xue Xue Bao*. 2010;45(11):1440–1446. Chinese.
21. Narang AS, Delmarre D, Gao D. Stable drug encapsulation in micelles and microemulsions. *Int J Pharm*. 2007;345(1–2):9–25. doi:10.1016/j.ijpharm.2007.08.057
22. Yang Q, Liu S, Gu Y, et al. Development of sulconazole-loaded nanoemulsions for enhancement of transdermal permeation and antifungal activity. *Int J Nanomedicine*. 2019;14:3955–3966. doi:10.2147/IJN.S206657
23. Nagai N, Ito Y. Therapeutic effects of gel ointments containing tranilast nanoparticles on paw edema in adjuvant-induced arthritis rats. *Biol Pharm Bull*. 2014;37(1):96–104. doi:10.1248/bpb.b13-00630
24. Wolfe MK, Wells E, Mitro B, et al. Seeking clearer recommendations for hand hygiene in communities facing ebola: a randomized trial investigating the impact of six handwashing methods on skin irritation and dermatitis. *PLoS One*. 2016;11(12):e0167378. doi:10.1371/journal.pone.0167378
25. Slaoui M, Bauchet AL, Fiette L. Tissue sampling and processing for histopathology evaluation. *Methods Mol Biol*. 2017;1641:101–114.
26. Changez M, Chander J, Dinda AK. Transdermal permeation of tetracaine hydrochloride by lecithin microemulsion: *in vivo*. *Colloid Surface B*. 2006;48(1):58–66. doi:10.1016/j.colsurfb.2006.01.007
27. Lopes LQ, Santos CG, de Almeida Vaucher R, et al. Ecotoxicology of glycerol monolaurate nanocapsules. *Ecotoxicol Environ Saf*. 2017;139:73–77. doi:10.1016/j.ecoenv.2017.01.019
28. Shen M, Liu C, Wan X, et al. Development of a daphnetin transdermal patch using chemical enhancer strategy: insights of the enhancement effect of Transcutol P and the assessment of pharmacodynamics. *Drug Dev Ind Pharm*. 2018;44(10):1642–1649. doi:10.1080/03639045.2018.1483391
29. Ali MS, Alam MS, Alam N, Siddiqui MR. Preparation, characterization and stability study of dutasteride loaded nanoemulsion for treatment of benign prostatic hypertrophy. *Iran J Pharm Res*. 2014;13(4):1125–1140.
30. Li W, Chen H, He Z, Han C, Liu S, Li Y. Influence of surfactant and oil composition on the stability and antibacterial activity of eugenol nanoemulsions. *Food Sci Technol*. 2015;62:39–47.
31. Su R, Yang L, Wang Y, et al. Formulation, development, and optimization of a novel octyldodecanol-based nanoemulsion for transdermal delivery of ceramide IIIB. *Int J Nanomedicine*. 2017;21(12):5203–5221. doi:10.2147/IJN.S139975
32. Joshi A, Joshi A, Patel H, Ponnoth D, Stagni G. Cutaneous penetration-enhancing effect of menthol: calcium involvement. *J Pharm Sci*. 2017;106(7):1923–1932. doi:10.1016/j.xphs.2017.03.041
33. Nagai N, Ogata F, Yamaguchi M, et al. Combination with l-menthol enhances transdermal penetration of indomethacin solid nanoparticles. *Int J Mol Sci*. 2019;20(15):3644. doi:10.3390/ijms20153644
34. Kunta JR, Goskonda VR, Brotherton HO, Khan MA, Reddy IK. Effect of menthol and related terpenes on the percutaneous absorption of propranolol across excised hairless mouse skin. *J Pharm Sci*. 1997;86(12):1369.
35. Dai X, Yin Q, Wan G, et al. Effects of concentrations on the transdermal permeation enhancing mechanisms of borneol: a coarse-grained molecular dynamics simulation on mixed-bilayer membranes. *Int J Mol Sci*. 2016;17(8):1349. doi:10.3390/ijms17081349
36. Lawrence MJ, Rees GD. Microemulsion-based media as novel drug delivery systems. *Adv Drug Deliv Rev*. 2000;45(1):89–121. doi:10.1016/S0169-409X(00)00103-4
37. Lane ME, Hadgraft J, Oliveira G, Vieira R, Mohammed D, Hirata K. Rational formulation design. *Int J Cosmet Sci*. 2012;34(6):496–501. doi:10.1111/j.1468-2494.2012.00747.x
38. Baspinar Y, Borchert HH. Penetration and release studies of positively and negatively charged nanoemulsions—is there a benefit of the positive charge? *Int J Pharm*. 2012;430(1–2):247–252. doi:10.1016/j.ijpharm.2012.03.040
39. Matsui T, Amagai M. Dissecting the formation, structure and barrier function of the stratum corneum. *Int Immunol*. 2015;27(6):269–280. doi:10.1093/intimm/dxv013